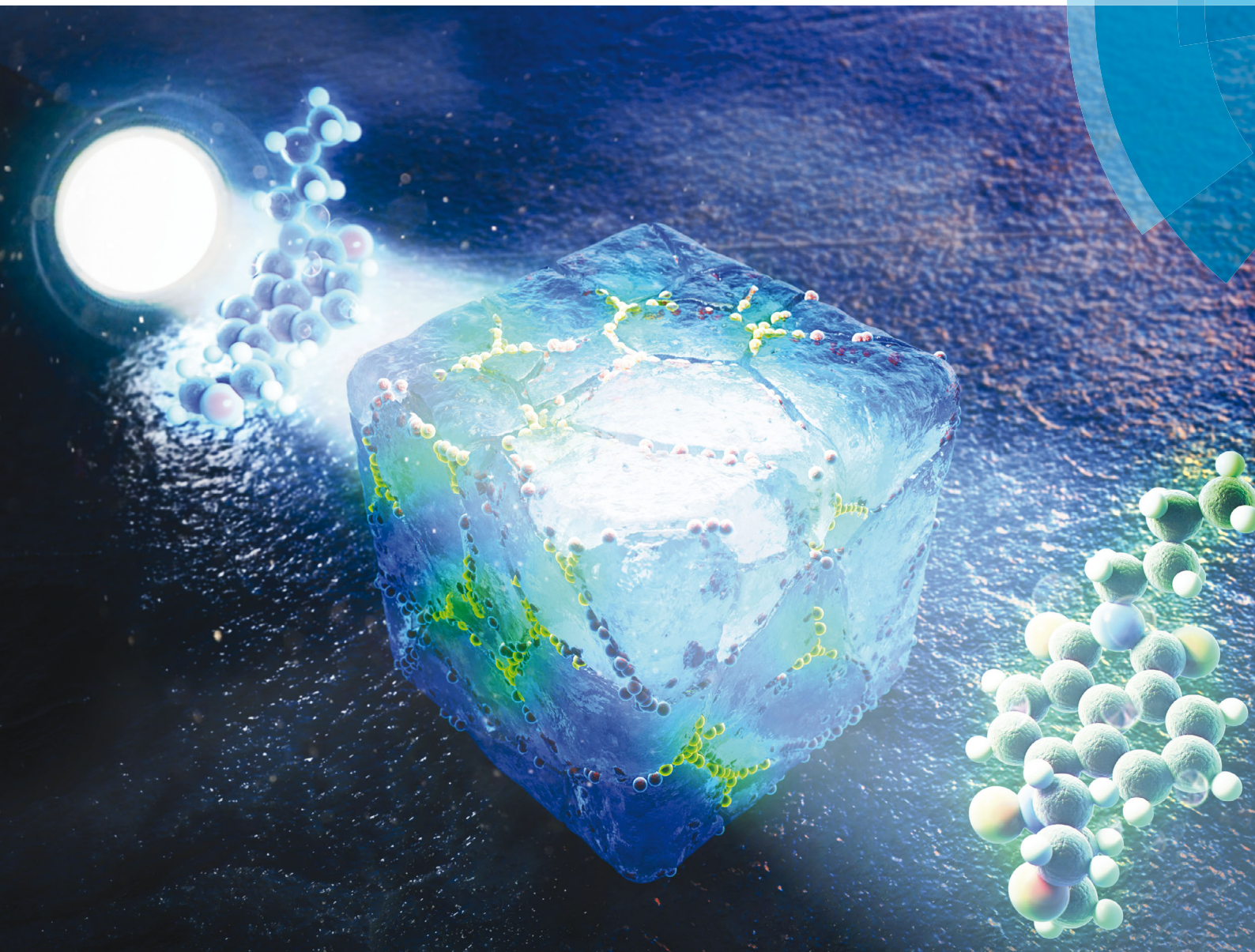


ChemComm

Chemical Communications

rsc.li/chemcomm



ISSN 1359-7345



ROYAL SOCIETY
OF CHEMISTRY

Celebrating
IYPT 2019

COMMUNICATION

Jong Seung Kim, Kitae Kim *et al.*

Enhanced sensitivity of fluorescence-based Fe(II) detection
by freezing



Enhanced sensitivity of fluorescence-based Fe(II) detection by freezing†

Cite this: *Chem. Commun.*, 2019, 55, 12136

Received 26th July 2019,
Accepted 3rd September 2019

DOI: 10.1039/c9cc05809e

rsc.li/chemcomm

Yun Hak Lee,^a Peter Verwilt,^b Hyeong Seok Kim,^b Jinjung Ju,^{ac}
Jong Seung Kim ^{*b} and Kitae Kim ^{*ad}

The first example of combining the fluorescent probe-based freeze concentration effect with *N*-oxide chemistry is reported for the highly sensitive and selective detection of ferrous ion (Fe(II)). Interestingly, our preliminary results demonstrated that the fluorescence intensity of Fe(II) was markedly enhanced upon freezing, and the location of Fe(II) in the freezing state was visualized by confocal microscopy using a cryostage.

Iron, a biologically abundant transition metal in living organisms, is widely distributed in nature, with some common sources including seawater, underground water, soil, and industrial waste.^{1,2} In particular, bioavailable iron (mainly Fe(II)) is regarded as a limiting factor for marine primary producers and phytoplankton growth in several oceans, including the Southern ocean.³ In nature, dissolved iron in water is mainly present in two redox states, namely the ferrous (Fe(II)) and ferric (Fe(III)) forms.⁴ Despite the universal distribution of iron, excessive or insufficient quantities of iron can cause significant issues to living organisms and the environment.⁵ As such, the quantity of iron in the biosphere should be maintained at an appropriate level, and so the accurate and precise detection of iron is the key to understanding the factors that regulate its concentration in nature.

Unlike in the case of industrial waste, the concentration of iron present in the natural water system generally ranges from 61 to 2680 ppm.⁶ In addition, although the accurate separation and measurement of divalent and trivalent iron ions is challenging, the selective detection of the more water soluble Fe(II) is necessary due to its importance in redox processes.⁷

Thus, to accurately and sensitively measure Fe(II), the quantitative and qualitative analysis of analytes can be achieved using atomic absorption spectroscopy (AAS), inductively coupled plasma mass spectrometry (ICP-MS), potentiometric stripping analysis (PSA), X-ray fluorescence (XRF), and radioisotopes.⁸ Since the above methods are expensive and sophisticated, a simple colorimetric method has been used as an alternative; however this is cumbersome and less selective. To overcome such issues, a rapid and accurate fluorescence method has been proposed for the detection of Fe(II), which allows the selective detection of certain substances present in the analytes.^{9,10}

In addition, in 2013, Nagasawa and co-workers reported the first turn-on fluorescent probe for the selective detection of Fe(II) using *N*-oxide chemistry in aqueous solution.¹¹ The installation of an *N*-oxide on the fluorophore induces fluorescence attenuation by twisted intramolecular transfer (TICT) and photo-induced electron transfer (PET). The oxidized dialkyl-arylamine moiety is selectively reduced by only Fe(II)-mediated deoxygenation, thereby resulting in a dramatic increase in fluorescence due to the recovery of π -conjugation in the fluorophore. Indeed, an *N*-oxide chemistry-based approach for the selective detection of Fe(II) has been widely employed in various biological applications.^{12–16} However, this method also has limitations since it has low sensitivity and low response rate to Fe(II) present in aqueous solutions.

To resolve this issue, a new fluorescence-based approach employing the freeze concentration effect was proposed. More specifically, Kim *et al.* reported that the freezing method increased the interactivity through the concentration of the various components in the quasi-liquid layer around the ice crystals, thereby significantly increasing the rate of the reaction compared to that in the liquid phase.¹⁷ This system has therefore aroused great interest in recent chemical and environmental studies. For example, a unique reaction between organic and inorganic matter takes place in a specific ice region accompanied by low pH conditions.^{18–21} More recently, this strategy has been applied by Choi *et al.* for investigating the degradation mechanism of organic pollutants.²²

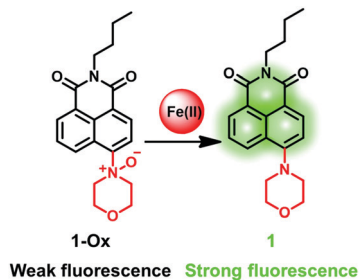
^a Korea Polar Research Institute (KOPRI), Incheon, 21990, Republic of Korea.
E-mail: ktkim@kopri.re.kr

^b Department of Chemistry, Korea University, Seoul, 02841, Republic of Korea.
E-mail: jongskim@korea.ac.kr

^c Department of Environmental Sciences and Biotechnology, Hallym University, Chuncheon, 24252, Republic of Korea

^d Department of Polar Sciences, University of Science and Technology (UST), Incheon, 21990, Korea

† Electronic supplementary information (ESI) available. See DOI: 10.1039/c9cc05809e



Scheme 1 Proposed reaction between the probe **1-Ox** and Fe(II).

Thus, we herein propose a novel idea based on the combination of the freeze concentration effect and *N*-oxide chemistry to sensitively and selectively detect Fe(II) (Scheme 1). More specifically, we report the design and synthesis of an Fe(II)-specific fluorescent probe (**1-Ox**) by the combination of a naphthalimide fluorophore and oxidized morpholine as an Fe(II)-selective reaction site (Scheme S1, ESI[†]). The proposed sensing mechanism of **1-Ox** with Fe(II) is based on the modulation of the intramolecular charge transfer (ICT) character of **1**, compared to the PET-quenched oxidized morpholine probe **1-Ox**, as supported by DFT calculations (Fig. S1 and S2, ESI[†]). The target compound, **1-Ox**, is synthesized according to a previously reported 3-step procedure with minor modifications, as shown in the ESI[†] (Scheme S1).²³ The identities of the newly synthesized compounds are confirmed by ¹H NMR, ¹³C NMR, and ESI-MS (ESI[†]).

To evaluate the response to Fe(II) and the effect of freezing, spectroscopic characterization of the probe **1-Ox** and its mother compound **1** was carried out. As shown in Fig. 1A, absorption bands with the maxima of 340 and 395 nm were found for **1-Ox** ($\epsilon = 1.3 \times 10^4 \text{ M}^{-1} \text{ cm}^{-1}$) and **1** ($\epsilon = 0.9 \times 10^4 \text{ M}^{-1} \text{ cm}^{-1}$), respectively. This indicates that a blue shift took place due to a less pronounced ICT character during the excitation, caused by the presence of the *N*-oxide moiety. Moreover, the quantum

yields (Φ_F) of **1** and **1-Ox** with an excitation at 360 nm were measured to be 0.31 and 0.02 (quinine sulphate as a standard), respectively (Table S1, ESI[†]).

In addition, **1-Ox** exhibited a weak emission band as a result of the PET quenching effect, while **1** exhibited a relatively strong fluorescence at 540 nm with an excitation at 395 nm (Fig. 1B). When **1-Ox** was treated with 1 equivalent of Fe(II) for 60 min, the fluorescence spectra showed negligible changes due to the low reactivity, in addition to the short reaction time (Fig. 1B). Based on the previous results for the combination of an Fe(II)-selective fluorescent probe with *N*-oxide chemistry, a reaction time of at least 60 min is required in addition to > 10 equivalents of Fe(II).¹²

To overcome this limitation, we introduced freezing and thawing methods for more efficient fluorescence detection. Preliminary experiments were carried out to determine the optimal conditions and the maximum freeze concentration effect was reached under buffer-free and slightly acidic conditions. As the reaction time of **1-Ox** with Fe(II) was increased from 0 to 60 min, the change in the fluorescence intensity at 25 °C was negligible (Fig. S3, ESI[†]). Upon extending the freezing time from 30 to 60 min, the fluorescence intensity of the mixture of **1-Ox** with Fe(II) increased significantly (Fig. S4, ESI[†]). The fluorescence intensity was then measured after thawing at 25 °C for 30 min (Fig. S5, ESI[†]). Furthermore, the fluorescence intensity of free **1-Ox** was found to be stable under freezing conditions up to 60 min (Fig. S6, ESI[†]) as well as under solution conditions at 25 °C (Fig. S7, ESI[†]).

Examination of the above results allowed us to determine that the freezing and thawing times of 30 min each were suitable. Using this novel analytical method, a mixture of **1-Ox** with 5 μM Fe(II) exhibited a remarkable 130-fold fluorescence enhancement upon freezing (30 min) compared to the previously reported results presented in Fig. 1C. Although the fluorescence intensity of free **1-Ox** also increased with scattering, a significantly greater enhancement in fluorescence (4 \times) was observed upon the addition of Fe(II). These results indicate that the fluorescence intensity increased due to the freeze concentration effect. In addition, Fig. 1D shows the fluorescence spectra of **1-Ox** after thawing in the absence and presence of Fe(II). Almost no fluorescence was observed for the free **1-Ox**, whereas the fluorescence intensity of **1-Ox** was increased up to 8-fold in the presence of Fe(II). This observation suggests that the deoxygenation reaction between **1-Ox** and 1 equivalent of Fe(II) was enhanced upon freezing.

The fluorescence response of **1-Ox** (5 μM) to Fe(II) over other metal ions was investigated under freezing and thawing conditions, where the fluorescence intensity at 540 nm is plotted in Fig. 2. The obtained results indicate that **1-Ox** can detect Fe(II) selectively over other metal ions. Likewise, none of the other tested biologically relevant reductants caused a notable change in the fluorescence intensity (Fig. S8, ESI[†]).^{11–14} Moreover, in the presence of ethylenediaminetetraacetic acid (EDTA) as an Fe(II) capping agent, a low fluorescence was observed, indicating that Fe(II) switched on the fluorescence. In addition, the fluorescence titration spectra of **1-Ox** with increasing concentrations of Fe(II) are shown in Fig. S9 (ESI[†]). Upon treatment with Fe(II), the

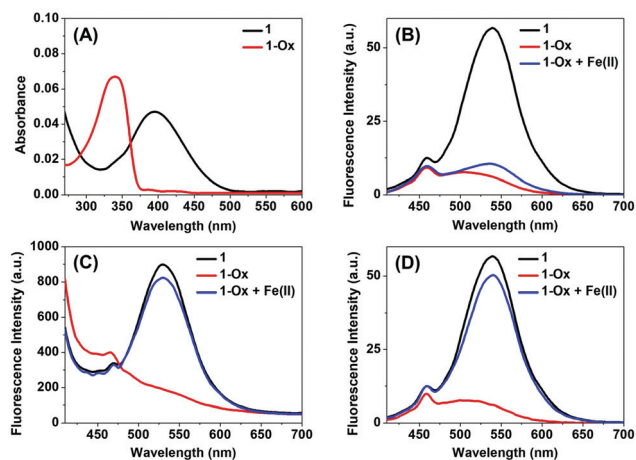


Fig. 1 (A) UV-vis absorption spectra of **1** (5 μM) and **1-Ox** (5 μM) in aqueous solution. Fluorescence spectra of **1** and **1-Ox** in the absence and presence of Fe(II) (5 μM) (B) at 25 °C for 60 min, and (C) under freezing (−20 °C) for 30 min, and (D) after thawing (25 °C) for 30 min in aqueous solution containing 0.5% (v/v) acetonitrile. Excitation was at 395 nm.

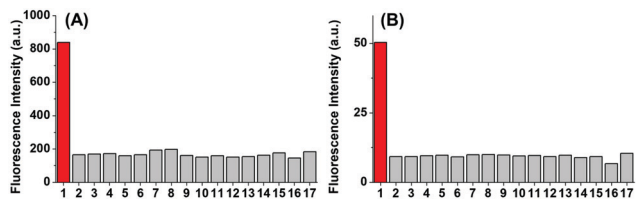


Fig. 2 Metal ion selectivity of **1-Ox** (5 μM) toward 5 μM of Fe(II) (1), 50 μM of various chloride salts (2 Fe(III); 3 Ba(II); 4 Co(II); 5 Cr(III); 6 Hg(II); 7 Cu(II); 8 Cu(I); 9 Ni(II); 10 Pb(II); 11 Zn(III); 12 Na(I); 13 K(I); 14 Mg(II); 15 Ca(II)), only **1-Ox** (16) and Fe(II) (5 μM) with 50 μM of EDTA (17), under (A) freezing conditions (-20 °C) for 30 min, and (B) after thawing (25 °C) for 30 min in aqueous solution containing 0.5% (v/v) acetonitrile. The results show the fluorescence intensities of **1-Ox** at 540 nm upon excitation at 395 nm.

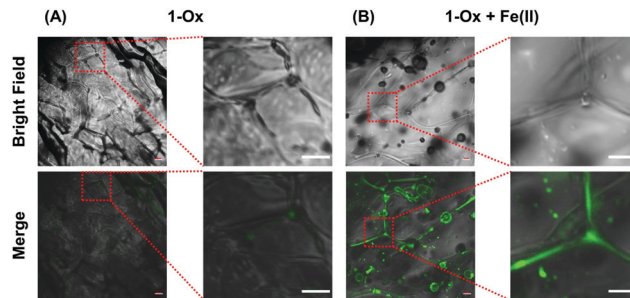


Fig. 4 Confocal microscopy images of **1-Ox** (5 μM) in the (A) absence and (B) presence of Fe(II) (5 μM) on the cryostage at -20 °C for 30 min. Merged images were obtained using the DIC and fluorescence images. The excitation and emission wavelengths were 405 and 450–600 nm, respectively. Scale bar = 20 μm.

fluorescence intensity of **1-Ox** at 540 nm gradually increased, reaching saturation around 5 μM under freezing and thawing conditions. The fluorescence response therefore demonstrates a linear relationship between the signal intensity and the Fe(II) concentration, allowing the detection limit to be determined as 0.27 μM under freezing and thawing conditions (Fig. S10, ESI†). However, a detection limit of 1.02 μM was obtained at 25 °C (Fig. S11, ESI†), thereby indicating that the freezing method is favorable for the detection of low concentrations of Fe(II).

As evident from HPLC analysis, the generation of **1** from the deoxygenation of **1-Ox** was induced by Fe(II) using the freezing method (Fig. 3). The retention time of **1** was observed to be 4.30 min upon excitation at 360 nm, whereas the peak of **1-Ox** was detected at 5.50 min. Upon the addition of Fe(II) to **1-Ox** under freezing and thawing conditions, the initial peak at 5.50 min almost disappeared, while a new peak was observed at 4.30 min, *i.e.*, at the same retention time as **1**. These results therefore confirm that Fe(II)-mediated deoxygenation took place to give **1** from **1-Ox**.

To visualize the accumulation of the probe in the liquid-like layer (LLL), freezing was carried out using a cryostage (Linkam FDCS196) and the localization was confirmed by confocal laser microscopy. As can be seen in Fig. S12 (ESI†), it shows the optical and fluorescence images of **1**, where accumulation was observed in ice. In addition, the fluorescence emission of **1-Ox** was found to be lower than that of **1** in the ice phase (Fig. 4A), while the fluorescence intensity of **1-Ox** in the presence of 1 equivalent of Fe(II) was significantly increased (Fig. 4B). In particular, the merged images show an overlap of fluorescence

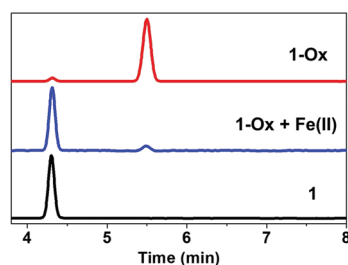


Fig. 3 HPLC analysis of **1** and **1-Ox** in the absence and presence of Fe(II) at a single wavelength (360 nm). The eluent was a binary mixture of a 0.1% phosphoric acid solution and acetonitrile (30 : 70 by volume) at a flow rate of 1.0 mL min⁻¹.

with differential interference contrast (DIC) from **1-Ox** with that of Fe(II), indicating that the probe settled in the LLL. Indeed, the magnification images confirm this in detail. Additional studies of these Z-stack images were then carried out for the probes, where the 3-dimensional images of **1-Ox** in the presence of Fe(II) (depth range = 0–80 μm) revealed evidence of localization in the LLL (Fig. S13, ESI†). It was therefore apparent that these microscopic images gave results similar to the spectroscopic data obtained in ice, thereby implying that the deoxygenation reaction occurred in the LLL.

Based on the promising imaging results obtained in ice, we also investigated the applicability of the **1-Ox** probe for the detection of Fe(II) generated by the freezing-enhanced chemical reaction in a cold environment. Indeed, Choi's group previously reported an enhancement in the reduction to Fe(II) from iron oxide in the presence of iodide ions in a frozen solution and its implication on iron bioavailability in cold environments.²⁴ Thus, the production of Fe(II) was carried out according to the previously reported procedures with minor modifications.²⁵ Prior to the application of **1-Ox** in an environmental system, free **1-Ox** and iron oxide were measured by confocal microscopy. A weak fluorescence in **1-Ox** was observed, whereas iron oxide was clearly concentrated in the LLL (Fig. 5). Moreover, the effect of iodide on the fluorescence change of **1-Ox** was negligible (Fig. S14, ESI†). When the iron oxide was pre-treated with iodide for 24 h at -20 °C and subsequently thawed at 25 °C and then incubated with **1-Ox** for 30 min at -20 °C, the fluorescence of **1-Ox** was significantly enhanced *via* production of Fe(II) from dissolution of iron oxide with iodide. These results indicate that **1-Ox** is a valuable tool not only for monitoring labile iron ions but also for understanding the accelerated chemical reaction in ice.

In conclusion, we designed and synthesized a novel Fe(II)-selective fluorescent probe, **1-Ox**, which is composed of naphthalimide and an oxidized morpholine moiety. Even in the presence of only 1 equivalent of Fe(II), the probe exhibited a highly sensitive fluorescence enhancement toward Fe(II) upon freezing as opposed to under 25 °C conditions. These results imply that an increased deoxygenation reactivity by Fe(II) in ice was closely related to the freeze concentration effect. Due to its favorable photophysical properties, **1-Ox** therefore appears to be a promising candidate for the sensitive detection of labile Fe(II) in environmental samples,

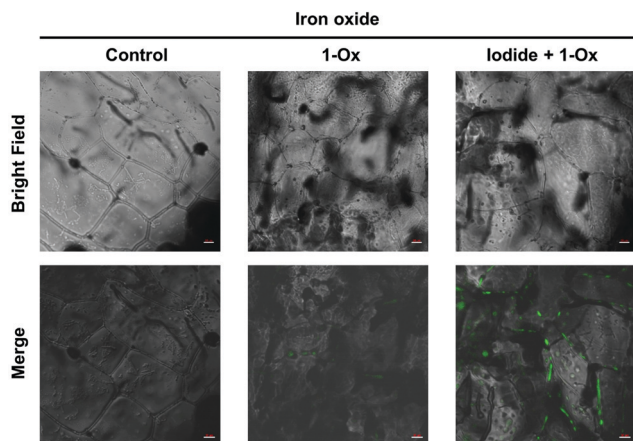


Fig. 5 Confocal microscopy images of iron oxide treated with **1-Ox** (5 μM) in the absence and presence of iodide on the cryostage at $-20\text{ }^{\circ}\text{C}$ for 30 min. Merged images were obtained from the DIC and fluorescence images. The excitation and emission wavelengths were 405 and 450–600 nm, respectively. Scale bar = 20 μm .

owing to a large Stokes shift, a low detection limit, and a high selectivity. As demonstrated by confocal laser microscopy, the addition of Fe(II) resulted in probe localization in the LLL in addition to an enhancement in fluorescence. As such, the combination of **1-Ox** with the appropriate freezing method demonstrates potential for application in the tracking of environmental Fe(II) in nature, and in particular in polar and cold environments. Furthermore, the reported combined strategy is described here for the first time, and we note that this method could be used to provide a better understanding of the environmental implications of Fe(II), while **1-Ox** could be considered a potential analytical tool for identification of the microstructure of ice.

This work was funded by the Korea Polar Research Institute (KOPRI) project (PE19200 to K. K.) and CRI project (2018R1A3B1052702 to J. S. K.) of the NRF of Korea.

Conflicts of interest

There are no conflicts to declare.

Notes and references

- 1 R. R. Crichton, S. Wilmet, R. Legssyer and R. J. Ward, *J. Inorg. Biochem.*, 2002, **91**, 9–18.
- 2 I. A. Mendelsohn, B. A. Kleiss and J. S. Wakeley, *Wetlands*, 1995, **15**, 37–46.
- 3 S. Wang and J. K. Moore, *J. Geophys. Res.*, 2011, **116**, C1019.
- 4 D. W. Domaille, E. L. Que and C. J. Chang, *Nat. Chem. Biol.*, 2008, **4**, 168.
- 5 K. Pantopoulos, S. K. Porwal, A. Tartakoff and L. Devireddy, *Biochemistry*, 2012, **51**, 5705–5724.
- 6 E. S. Gurzau, C. Neagu and A. E. Gurzau, *Ecotoxicol. Environ. Saf.*, 2003, **56**, 190–200.
- 7 W. Breuer, M. Shvartsman and Z. I. Cabantchik, *Int. J. Biochem. Cell Biol.*, 2008, **40**, 350–354.
- 8 S. M. Pyle, J. M. Nocerino, S. N. Deming, J. A. Palasota, J. M. Palasota, E. L. Miller, D. C. Hillman, C. A. Kuharic, W. H. Cole and P. M. Fitzpatrick, *Environ. Sci. Technol.*, 1995, **30**, 204–213.
- 9 A. T. Aron, A. G. Reeves and C. J. Chang, *Curr. Opin. Chem. Biol.*, 2018, **43**, 113–118.
- 10 W. Xuan, R. Pan, Y. Wei, Y. Cao, H. Li, F.-S. Liang, K.-J. Liu and W. Wang, *Bioconjugate Chem.*, 2015, **27**, 302–308.
- 11 T. Hirayama, K. Okuda and H. Nagasawa, *Chem. Sci.*, 2013, **4**, 1250–1256.
- 12 T. Hirayama, H. Tsuboi, M. Niwa, A. Miki, S. Kadota, Y. Ikeshita, K. Okuda and H. Nagasawa, *Chem. Sci.*, 2017, **8**, 4858–4866.
- 13 T. Hirayama, M. Inden, H. Tsuboi, M. Niwa, Y. Uchida, Y. Naka, I. Hozumi and H. Nagasawa, *Chem. Sci.*, 2019, **10**, 1514–1521.
- 14 M. Niwa, T. Hirayama, I. Oomoto, D. O. Wang and H. Nagasawa, *ACS Chem. Biol.*, 2018, **13**, 1853–1861.
- 15 G. Liu, W. Chen, Z. Xu, F. Ye, Y. Pan, X. Chen, S. H. Liu, L. Zeng and J. Yin, *Org. Biomol. Chem.*, 2018, **16**, 5517–5523.
- 16 G. Liu, X. Han, J. Zhang, Z. Xu, S. H. Liu, L. Zeng and J. Yin, *Dyes Pigm.*, 2018, **148**, 292–297.
- 17 K. Kim, W. Choi, M. R. Hoffmann, H.-I. Yoon and B.-K. Park, *Environ. Sci. Technol.*, 2010, **44**, 4142–4148.
- 18 K. Kim, H. Y. Chung, J. Ju and J. Kim, *Sci. Total Environ.*, 2017, **590**, 107–113.
- 19 J. Ju, J. Kim, Ľ. Vetráková, J. Seo, D. Heger, C. Lee, H.-I. Yoon, K. Kim and J. Kim, *J. Hazard. Mater.*, 2017, **329**, 330–338.
- 20 D. Jeong, K. Kim and W. Choi, *Atmos. Chem. Phys.*, 2012, **12**, 11125–11133.
- 21 K. Kim and W. Choi, *Environ. Sci. Technol.*, 2011, **45**, 2202–2208.
- 22 Y. Choi, H.-I. Yoon, C. Lee, L. Vetráková, D. Heger, K. Kim and J. Kim, *Environ. Sci. Technol.*, 2018, **52**, 5378–5385.
- 23 P.-Y. Gu, C.-J. Lu, Z.-J. Hu, N.-J. Li, T.-T. Zhao, Q.-F. Xu, Q.-H. Xu, J.-D. Zhang and J.-M. Lu, *J. Mater. Chem. C*, 2013, **1**, 2599–2606.
- 24 S. P. M. Menacherry, K. Kim, W. Lee, C. H. Choi and W. Choi, *Environ. Sci. Technol.*, 2018, **52**, 13766–13773.
- 25 K. Kim, S. P. M. Menacherry, J. Kim, H. Y. Chung, D. Jeong, A. Saiz-Lopez and W. Choi, *Environ. Sci. Technol.*, 2019, **53**, 7355–7362.